

Check for updates

Revealing Rate-Determining Factors of Interfacial Lithium-Ion Transport for Efficient Membrane Lithium Separation

Xiangming Yao, Shiming Chen, Hengyao Zhu, Wenguang Zhao, Bowen Nan, Hai Lin, Yongli Song,* Huanting Wang,* Luyi Yang,* and Feng Pan*

Extracting lithium from seawater, which contains 70% of global lithium reserves, is highly critical for the sustainable development of lithium-ion batteries. However, low concentration of lithium-ion (Li⁺) and abundant interfering cations in seawater requires highly selective and efficient Li+ transport at the solid-liquid interface. In this study, key factors influencing interfacial Li+ transport across the surface of a perovskite solid-state electrolyte are investigated, including surface hydrophilicity, Li+ concentration, and interfering ions. The solvation structure of lithium ions at the interface and near-surface regions is examined using depth-profiling Raman spectroscopy for the first time. It is revealed that a surface with lower hydrophilicity reduces the hydration degree of Li⁺ at the surface, resulting in lower desolvation energy, which in turn promotes Li⁺ conduction at the solid-liquid interface. Similarly, increasing Li+ concentration or the presence of other cations with high hydration capability will also promote the de-solvation of Li+. By unveiling the rate-limiting factors of Li+ transport at liquid-solid interfaces, this study offers valuable insights for designing practical lithium extraction membranes.

1. Introduction

In recent years, lithium (Li) has emerged as a strategically significant commodity accompanied by the development of advanced portable devices and electric vehicles.^[1,2] Current commercial Li is mainly from salt-lake brines and high-grade ores which is unable to meet the increasing Li consumption (it has been projected with a compound annual growth rate of 20% over coming decades).^[3] At this long-term trend, the residual Li reserve on land will be exhausted by 2080. Hence, extracting Li from the

seawater has become an important way to maintain the sustainable and sound industrial growth of lithium battery, which contains $\approx\!16$ 400 times more Li than is found in the earth's crust. [4] However, the dilute Li concentrations ($\approx\!0.17$ mg L $^{-1}$) and high concentration of interfering ions (i.e., Na $^{+}$, Mg $^{2+}$, and K $^{+}$) are two main difficulties for Li extraction. [4.5]

Nowadays, some novel methods have been proposed to extract Li from seawater, including adsorption,[6,7] liquidextraction,[8-10] electrochemical extraction, [5,11] and electrodialysis. [12,13] In terms of separation, membrane separation methods are energy conservation and environment protection methods which have been widely used for preconcentration and Li extraction. However, conventional nanofiltration processes exhibit low selectivity of Li+/Na+ and suffer from severe inorganic scaling.[14,15] Alternatively, electrodialysis through ion exchange membranes (e.g., organics

impregnated with ionic liquid and solid-state electrolyte) is efficient for metal ions separation. [16,17] It is worth noting that the membrane should be thin to enable ultrafast ion transport but mechanically robust to maintain stable performances. For instance, Lai et al. applied glass-type $\text{Li}_{0.33}\text{La}_{0.57}\text{TiO}_3$ (LLTO) membrane to separate Li^+ and other interfering ions, [18] realizing stable Li extraction.

To this date, most studies have focused on ${\rm Li^+}$ transport within the membrane, while few have investigated the solvation structure and properties of the solid-liquid interface. It should

X. Yao, S. Chen, W. Zhao, B. Nan, H. Lin, L. Yang, F. Pan School of Advanced Materials Peking University Shenzhen Graduate School Shenzhen 518055, P. R. China E-mail: yangly@pkusz.edu.cn; panfeng@pkusz.edu.cn H. Zhu Department of Chemistry

City University of Hong Kong Kowloon 999077, Hong Kong

The ORCID identification number(s) for the author(s) of this article can be found under https://doi.org/10.1002/adfm.202426072

DOI: 10.1002/adfm.202426072

Y. Song School of Energy and Power Engineering Jiangsu University Zhenjiang 212013, China E-mail: songyl@ujs.edu.cn

H. Wang

Department of Chemical Engineering Monash University Clayton

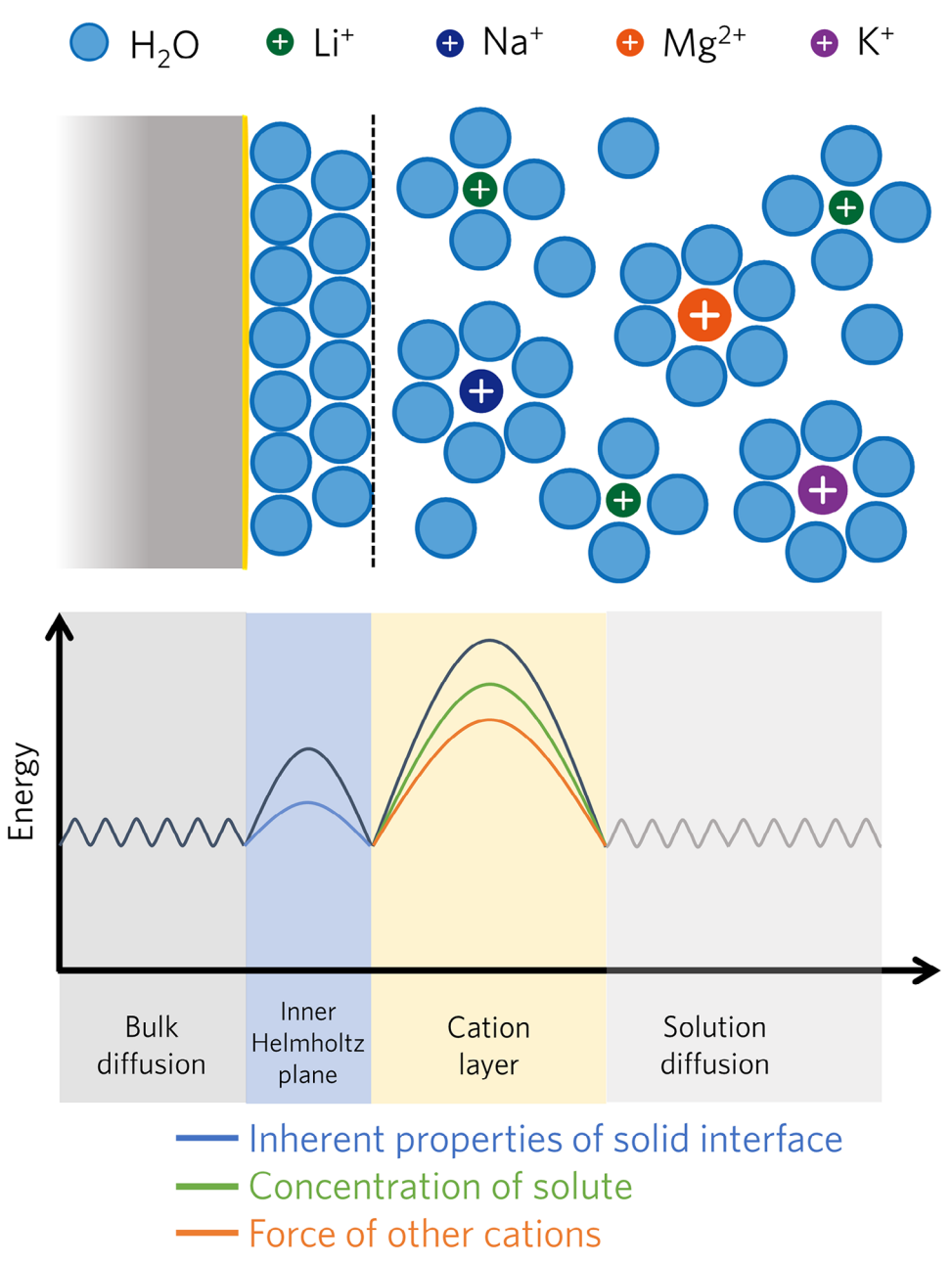
Victoria 3800, Australia

E-mail: huanting.wang@monash.edu

onlinelibrary. wiley.com/doi/10.1002/adfm.202426072 by University Town Of Shenzhen, Wiley Online Library on [18/11/2025]. See the Terms

nditions) on Wiley Online Library for rules of use; OA articles are governed by the applicable Creative Commons License

www.afm-journal.de



Scheme 1. Schematic illustration of the various factors influencing interfacial Li+ transport from aqueous solutions to solid electrolytes.

be noted that, during the Li extraction process, solvating $\rm H_2O$ molecules must be completely removed before Li⁺ can enter the membrane. This step consumes a significant amount of energy, thereby impeding the transport of Li⁺.[11] Therefore, understanding the de-solvation behaviors of Li⁺ at the interface is crucial.[19,20] The Li⁺ de-solvation process at the interface depends significantly on two primary factors: first, the structure of the solvation sheath in the bulk solution determines the inherent de-solvation energies of Li⁺;[21,22] second, the affinity between the solvent (i.e., $\rm H_2O$) and the membrane governs the concentration of solvents at the interface, thereby influencing the Li⁺ de-solvation process.[23,24] Therefore, conducting a systematic study on these factors is crucial for developing a

comprehensive understanding of the interfacial ${\rm Li^+}$ transport process.

As demonstrated in **Scheme 1**, in this work, we have investigated the interface Li⁺ transport process of a perovskite solid-state electrolyte (LITO) through combining depth-profiling and in situ Raman spectra. First, by applying an exterior glass phase ($45\text{Li}_2\text{O}-42\text{B}_2\text{O}_3-13\text{SiO}_2$, denoted as LBSO) coating layer, the interfacial affinity with H₂O is tuned. It is revealed that constructing a relatively hydrophobic interface could reduce the interfacial water enrichment in the inner Helmholtz plane and improve the de-solvation rate of Li⁺, facilitating highly selective and rapid Li extraction. Next, the coordination environment of interfacial H₂O molecules is studied with various Li⁺ concentrations and

16163028, 2025, 38, Downloaded from https://advanced.onlinelibrary.wiley.com/doi/10.1002/adfm.202426072 by University Town Of Shenzhen, Wiley Online Library on [18/11/2025]. See the Terms

nditions) on Wiley Online Library for rules of use; OA articles are governed by the applicable Creative Commons License

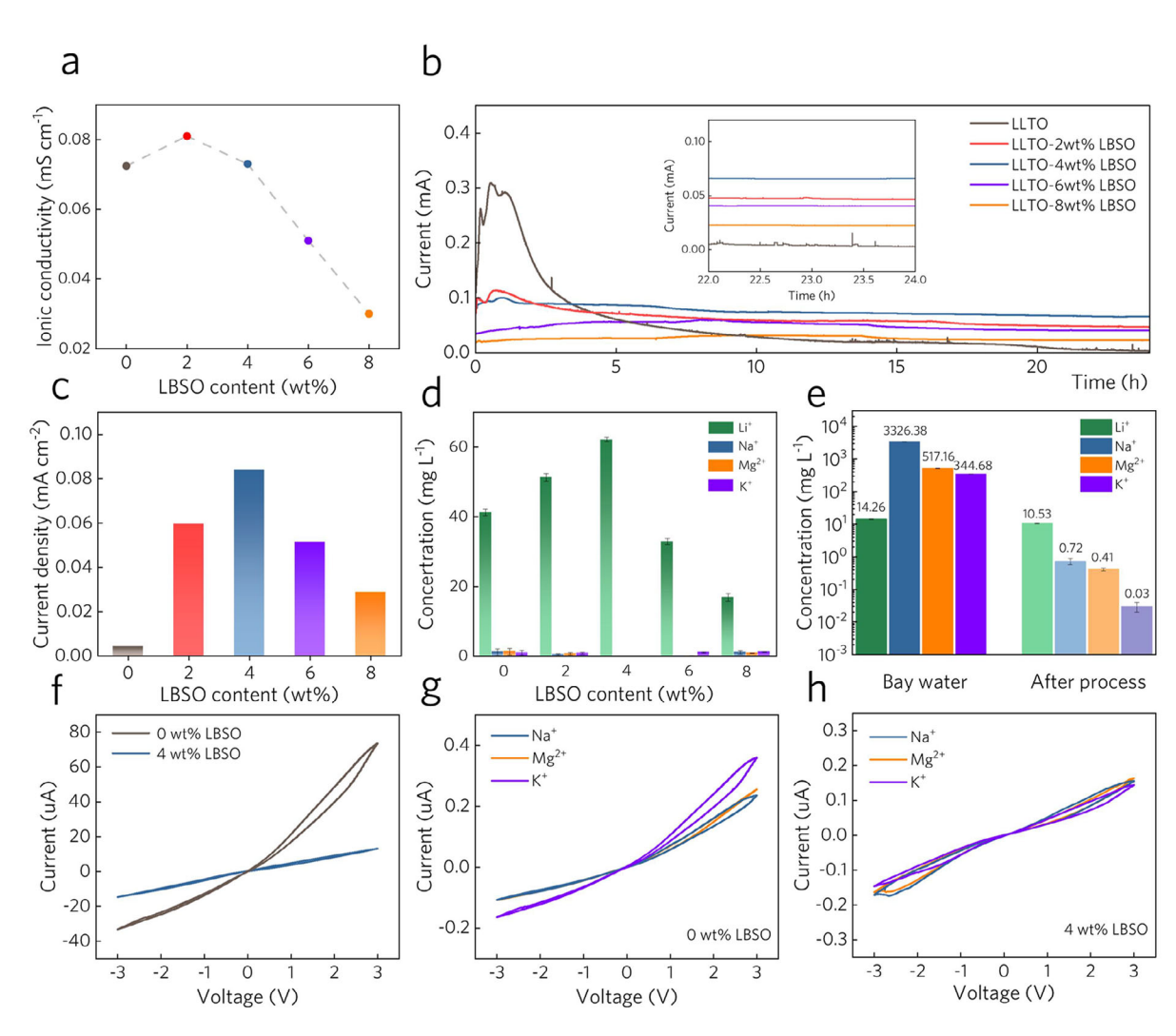


Figure 1. a) Ionic conductivity of LLTO with different content of LBSO; b) Current curves of lithium separation tests for LLTO with various LBSO contents; c) Steady-state current of lithium separation tests; d) Elemental content of the extract from lithium separation tests; e) Comparison of ion concentrations of bay water and extract solution after 5 h test using LLTO-4%LBSO as cation exchange membrane; f) CV curves of systems using LLTO or LLTO-4%LBSO as cation exchange membrane in the 1 mol L^{-1} LiCl solution; CV curves of systems using LLTO g) or LLTO-4%LBSO h) as cation exchange membrane in other cation solutions (1 mol L^{-1} NaCl, 1 mol L^{-1} MgCl₂ and 1 mol L^{-1} KCl).

interfering cations (Na⁺, Mg²⁺, and K⁺). On the one hand, a higher Li salt concentration would lead to a lower average Li⁺ solvation number; on the other hand, the introduced cations could preferentially solvate with $\rm H_2O$ molecules, weakening the bonding strength between Li⁺ and $\rm H_2O$. By revealing the rate-determining factors of Li⁺ transport at the interface between aqueous solution and solid-state electrolytes, this study provides important insights for the design of practical Li extraction membranes.

2. Results and Discussion

2.1. Li⁺ Separation Performance

To investigate the effect of LBSO incorporation on LLTO, we first measured the XRD patterns of LLTO with varying amounts of LBSO (Figure S1, Supporting Information). It can be observed from the TEM images (Figure S2, Supporting Information) that after high-temperature co-sintering, LBSO forms a uniform coating layer on the surface of LLTO. In this case, the introduction of LBSO does not alter the crystal structure of LLTO, ensuring the electrolyte membrane retains its Li+ conductivity. The electrochemical impedance spectra results (Figure S3, Supporting Information) show that the LLTO with 2 wt% LBSO exhibits the highest ionic conductivity (Figure 1a). Based on the electron back scatter diffraction (EBSD) results (Figure \$4, Supporting Information), this improvement could be attributed to the improved contact of LLTO at inter-grain boundaries, where LBSO serves as a "binding agent" (Figure S5, Supporting Information). [25] The higher macroscopic density of LLTO with LBSO also indicates a reduction in grain boundaries, thereby improving the ion selectivity (Figure S6, Supporting Information). The energy dispersive spectra (EDS) also confirm the homogeneous

16163028, 2025, 38, Downloaded from https://advanced.onlinelibrary.wiley.com/doi/10.1002/adfm.202426072 by University Town Of Shenzhen, Wiley Online Library on [18/11/2025]. See the Terms and Conditions (https://onlinelibrary.wiley.com/terms

and-conditions) on Wiley Online Library for rules of use; OA articles are governed by the applicable Creative Commons License

www.afm-journal.de

distribution of LBSO within the LLTO pellet (Figure S7, Supporting Information). As the amount of LBSO added increases, the ionic conductivity of the membrane decreases, eventually falling below that of pristine LLTO. This decline is likely due to the low intrinsic ionic conductivity of LBSO.

To study the effect of different LBSO contents on the Li separation efficiency, potentiostatic measurements were carried out with LLTO with various LBSO contents (Figure 1b) in a Htype electrochemical cell (shown in Figure S8, Supporting Information). Although it does not have the highest ion conductivity, the membrane with 4 wt% LBSO exhibited the highest steady-state current (Figure 1c) as well as the highest Li separation efficiency (Figure 1d). Therefore, it can be speculated that there may be other factors influencing the Li separation performance. Furthermore, we conducted seawater Li extraction tests using LLTO with 4 wt% LBSO (denoted as LLTO-4%LBSO). The results showed that after operating for 5 h under a 5 V voltage (Figure S9, Supporting Information), the Mg2+/Li+ ratio in the obtained solution was reduced by 931 times compared to that in the bay water (Figure 1e), demonstrating the significant potential for Li mining from seawater. Similar results were found in the prepared solution system which contains the same composition of seawater (Figure \$10, Supporting Information). By analyzing the cyclic voltammogram (CV) curves of LLTO-4%LBSO and pristine LLTO pellet (Figure 1f), it can be observed that the CV curve of the former is symmetric, while the latter exhibits a distinct relaxation phenomenon. This relaxation may be due to the accumulation of Li+ at the interface of LLTO. From this, it can be inferred that the LBSO coating can alter the transport behavior of Li+ at the interface. Additionally, similar phenomena can be observed for other selected ions (Figure 1g,h).

2.2. Influence of Solid Interface

To study the impact of the electrolyte-liquid interface on Li⁺ desolvation behavior, we first analyzed the Li+-H2O structure in the inner Helmholtz plane under static conditions using depth-profiling Raman spectroscopy (see the schematic setup in Figure S11, Supporting Information). [26] By measuring the disappearance position of the Raman peak corresponding to the Ti-O bond vibration along the c-axis (553.4 cm⁻¹), we can identify the solid-liquid interface (Figure S12, Supporting Information).[27] Significantly intensified peaks corresponding to the O-H stretching modes of H_2O (3155 and 3350 cm⁻¹) and the vibration modes of interactions between H₂O and Li⁺ (3540 cm⁻¹) were detected near the interface of pristine LLTO pellet (Figure 2a). [28] By sharp contrast, the above peaks became weaker near the surface of LLTO-4%LBSO (Figure 2b). The above results show that solvated Li⁺ is enriched on the surface of LLTO, indicating a stronger Li⁺-H₂O coordination; however, when the surface is coated with LBSO, solvated Li-ions tend to move away from the interface. Besides, depth-profiling Raman spectra of LLTO with 2 wt% LBSO were also studied (Figure S13, Supporting Information). It is worth noting that intensified peaks corresponding to the H₂O and the interactions between H2O and Li+ were observed near the solid surface compared with LLTO-4%LBSO, which is consistent with the performance trends observed in electrochemical lithium extraction. Therefore, it can be speculated that under the premise of similar solid electrolyte interphase conductivity, the solvation structure at the interface plays a more significant role. To verify the experimental data, ab-initio molecular dynamics (AIMD) was further carried out to simulate the interfaces of LLTO and two different structural units in LBSO (represented by LiBSiO₄ and LiBO₂) with the solution. The simulations revealed that each Li+ at the LLTO interface is coordinated with 4 H₂O molecules; whereas at the LiBSiO₄ interface, the coordination number is only 3 (Figure 2c; Figures S14 and S15, Supporting Information), which agrees with the depth-profiling Raman spectra. The energy barriers associated with the Li⁺-4H₂O de-solvation process show that a lower number of coordinated H₂O molecules correlates with a reduced interfacial de-solvation energy barrier for Li⁺, thereby facilitating an easier de-solvation process (Figure \$16, Supporting Information).^[29] Additionally, the radial distribution functions (RDF) curves indicate that the Li+-H2O coordination distance for solvated Li+ at the LLTO interface (1.88 Å) is shorter compared to that of LiBSiO₄ (2.05 Å) (Figure 2c), further confirming a weakened Li⁺-H₂O interaction on LSBO.

Next, in order to unveil the origin of different interfacial Li⁺-H₂O coordinating behaviors, density functional theory (DFT) calculations of the binding energy between different surfaces with H₂O were performed (Figure 2d). The results show that LLTO surface exhibits a much higher binding energy with H₂O (-2.55 eV) than that of LiBO₂ (-1.10 eV) and LiBSiO₄ (-0.80 eV). The DFT results are supported by the contacting angles measurements (Figure \$17, Supporting Information), where the contact angles between de-ionized water and electrolyte pellets increase with the amount of LBSO. Both experimental and computational evidence indicate that the LLTO surface becomes less hydrophilic after LBSO modification. Therefore, the impact of the surficial structure of solid electrolyte membrane on interfacial ion solvation structure is illustrated in Figure 2e: a highly hydrophilic solid surface is more likely to result in a H₂O-rich solvation structure for Li⁺ at the interface, hence higher desolvation energy; by applying a thin coating layer with moderate hydrophilicity tend to form a H2O-deficient solvation structure at the solid-liquid interface, kinetically favoring the Li⁺ desolvation

To further demonstrate the impact of different solid phase interfaces on the Li⁺ desolvation process, in situ, Raman analysis on the solid-liquid interface was carried out, as illustrated in Figure \$18 (Supporting Information). We found that for pristine LLTO, the Raman peaks corresponding to the O-H stretching modes of H₂O (3155 and 3350 cm⁻¹) and the vibrational modes of Li⁺-H₂O interactions (3540 cm⁻¹) increased continuously under the biased voltage (Figure 3a). This indicates a significant accumulation of solvated Li+ in the inner Helmholtz plane. In contrast, for LLTO-4%LBSO, the changes in peak intensities during voltage application were relatively minor in the inner Helmholtz plane. It is reasonable to speculate that the suppressed accumulation of solvated Li⁺ at the interface is also due to the lower desolvation energy for Li+. Considering that the ion conductivities of LLTO and LLTO-4%LBSO are very similar (Figure 1a), the significant current change and the relatively lower steady-state current observed with pristine LLTO (Figure 3b) can be attributed to the hindered desolvation rate at

16163028, 2025, 38, Downloaded

mlinelibrary.wiley.com/doi/10.1002/adfm.202426072 by University Town Of Shenzhen, Wiley Online Library on [18/11/2025]. See the Terms

on Wiley Online Library for rules of use; OA articles are governed by the applicable Creative Commons

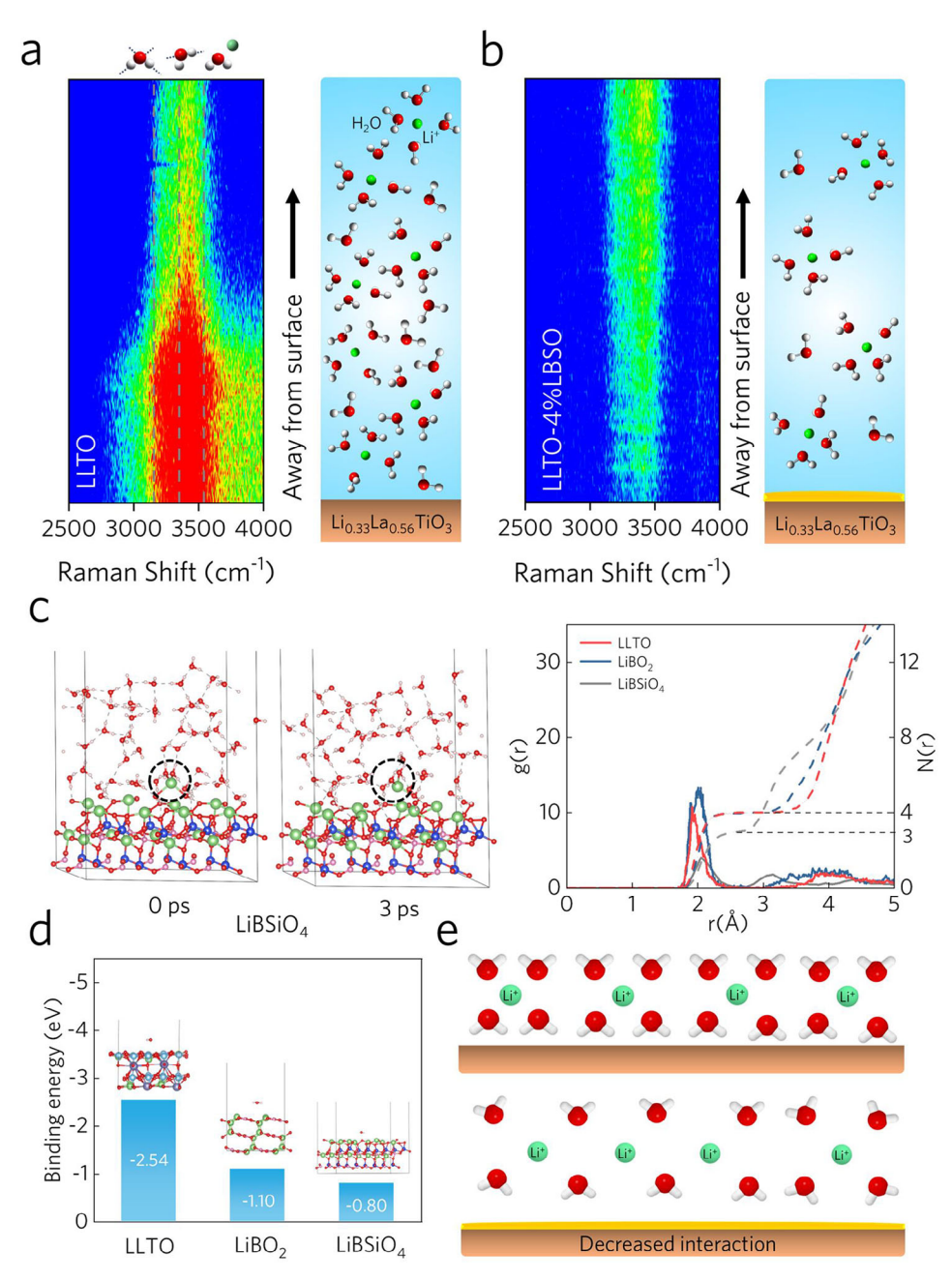


Figure 2. Depth-profiling Raman spectra of LLTO a) and LLTO-4%LBSO b) in the 1 mol L^{-1} LiCl aqueous solution (the test depth is \approx 5 μ m and chemical diagrams are H_2O or Li^+); c) Screenshots of AIMD simulation for LiBSiO₄ in the 1 mol L^{-1} LiCl aqueous solution (left); Radial distribution functions (RDF) and corresponding coordination numbers (N(r)) of Li^+ -O (H_2O) in the 1 mol L^{-1} LiCl aqueous solution; d) Binding energy between different solid interfaces and H_2O ; e) Schematic illustration of different solid surface for interfacial water cluster structure.

the LLTO surface (Figure 3c), causing concentration polarization resistance for Li⁺ at the interface. This phenomenon also explains the relaxation observed in the CV curves of the cell using LLTO (Figure 1f). In comparison, as illustrated in Figure 3c, the higher steady-state current and the small current change measured in the cell using LLTO-4%LBSO indicates that the less hydrophilic LBSO surface not only accelerates the Li⁺ desolvation process but also avoids accumulation of solvated Li⁺ at the solid-liquid interface.

2.3. Influence of Solute Concentration

In addition to the inherent properties of the solid surface, various solution compositions (i.e., lithium salt concentration and other cations) can also affect the Li⁺ desolvation process. It has been widely reported that the concentration of Li⁺ is another key variable that dictates the desolvation energy.^[30] Therefore, in this section, we studied the desolvation behavior of Li⁺ at the solid-liquid interface under two different concentrations of LiCl. It

www.advancedsciencenews.com

16163028, 2025, 38, Downloaded from https://advanced.

onlinelibrary.wiley.com/doi/10.1002/adfm.202426072 by University Town Of Shenzhen, Wiley Online Library on [18/11/2025]. See the Terms

nditions) on Wiley Online Library for rules of use; OA articles are governed by the applicable Creative Commons

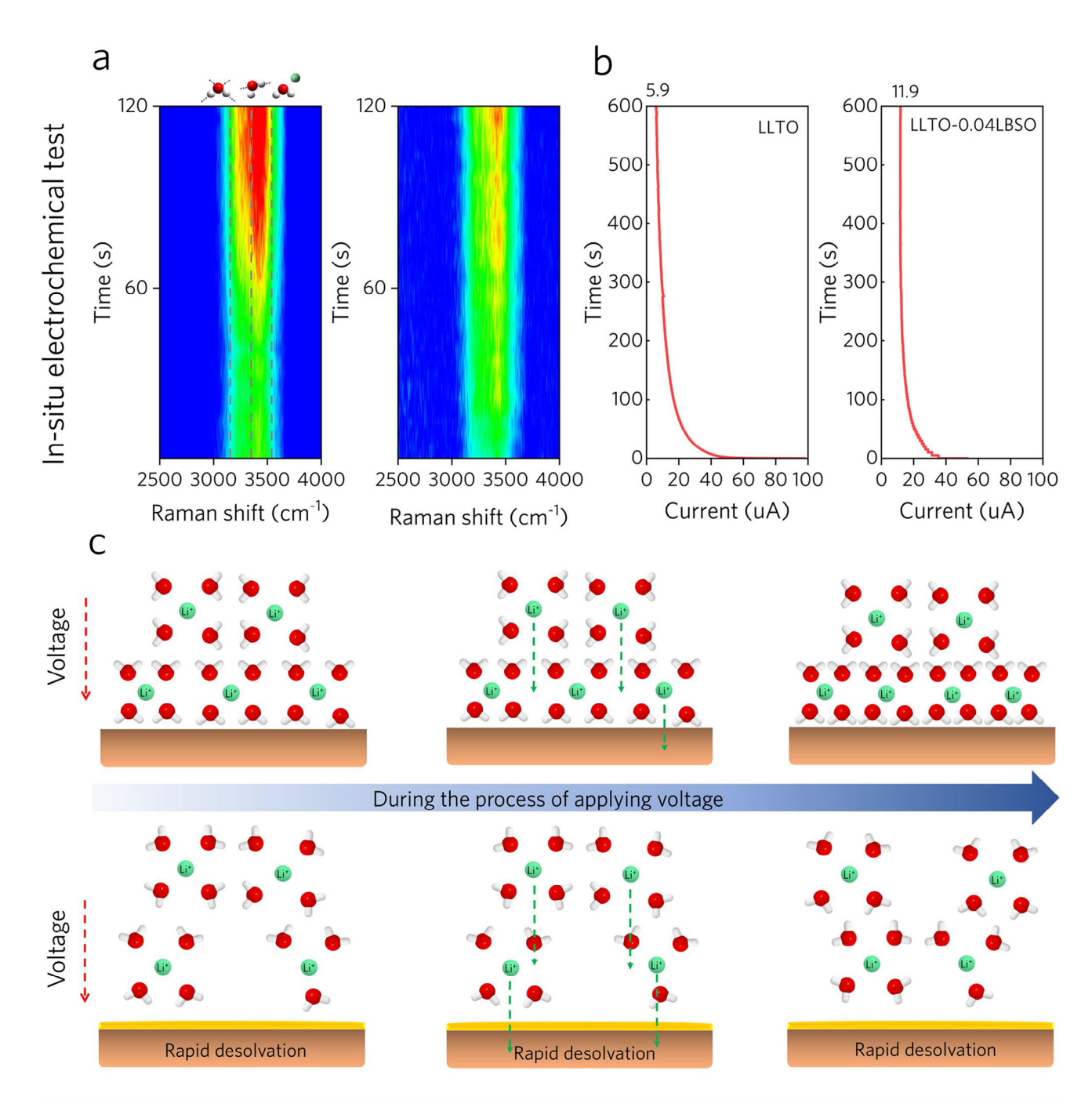


Figure 3. a) In situ electrochemical Raman spectra of LLTO and LLTO-4%LBSO in the 1 mol L⁻¹ LiCl aqueous solution with a 5 V forward voltage; b) Current-time curves of LLTO and LLTO-4%LBSO during the In situ electrochemical Raman spectra test; c) Schematic illustration of different solid surface for interfacial water cluster structure after the application of voltage.

is found that the corresponding current slightly increased with the Li⁺ concentration (Figure 4a). More importantly, compared to the cell with a lower LiCl concentration (1 M), the cell with a higher concentration (4 м) exhibited a more reversible curve, while the former still showed a small relaxation loop. According to the above results, it can be inferred that an increase in Li⁺ concentration enables a facile desolvation process at the interface. To validate this speculation, we conducted depth-profiling Raman measurements using a pure LLTO pellet (Figure 4b). Compared to Figure 2a, the Raman peak intensities corresponding to the O-H stretching modes of H₂O (3155 and 3350 cm⁻¹) and the vibrational modes of Li⁺-H₂O interactions (3540 cm⁻¹) were weaker in the 4 M LiCl solution. Additionally, the Raman signal layer corresponding to the accumulation of solvated Li⁺ at the interface was narrower. To explore the mechanism behind this phenomenon, we conducted molecular dynamics simulations of different

16163028, 2025, 38, Downloaded

.com/doi/10.1002/adfm.202426072 by University Town Of Shenzhen, Wiley Online Library

nditions) on Wiley Online Library for rules of use; OA articles are governed by the applicable Creative Commons

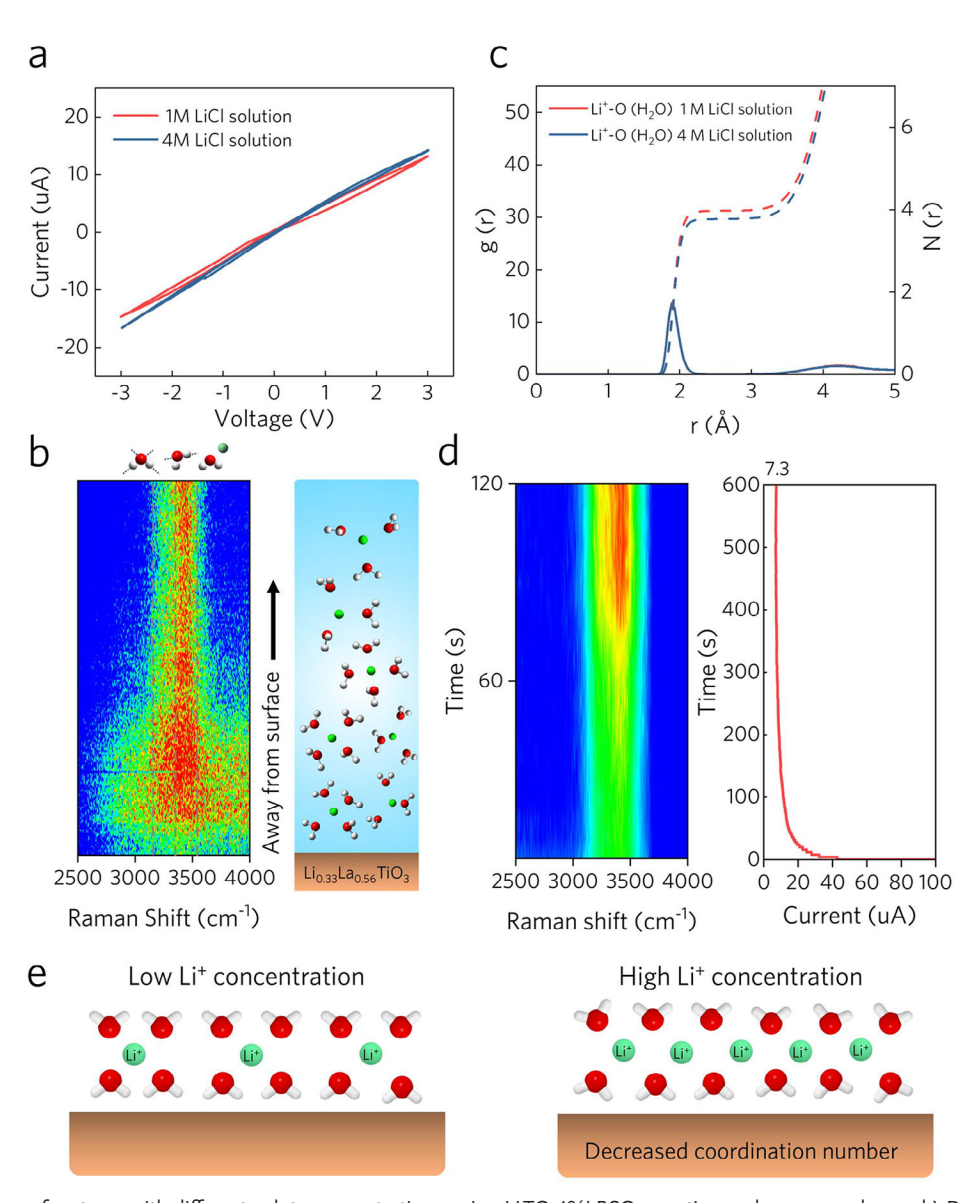


Figure 4. a) CV curves of systems with different solute concentrations using LLTO-4%LBSO as cation exchange membrane; b) Depth-profiling Raman spectra of LLTO in the 4 mol L^{-1} LiCl aqueous solution (the test depth is $\approx 5 \, \mu m$ and chemical diagrams are H_2O or Li^+); c) RDF and corresponding coordination N(r) of different solute concentration aqueous solution; d) In situ electrochemical Raman spectra of LLTO in the 4 mol L^{-1} LiCl aqueous solution with a 5 V forward voltage; e) Schematic illustration of different solute concentration for interfacial water cluster structure.

solutions (Figure 4c). The results showed that as the Li⁺ concentration increased from 1 to 4 M, the coordination number of Li⁺ in the solvent decreased from 3.97 to 3.77, indicating a weakened Li⁺-H₂O solvation as more Cl⁻ entered the first solvation sheath of Li⁺. The peak shift toward a lower chemical shift in ^7Li NMR spectra (Figure S19, Supporting Information) in the 4 M LiCl solution also confirms the stronger screening effect due to the formation of more contact ion pairs. [31]

Moreover, in situ electrochemical Raman spectra (Figure 4d) also showed that, compared to Figure 3a, the accumulation of solvated ${\rm Li^+}$ at the solid-liquid interface was alleviated in the solution with 4 M LiCl under biased voltage. This result indicates that a lower ${\rm H_2O}$ coordination number of ${\rm Li^+}$ leads to a lower desolvation energy, hence the faster interfacial ${\rm Li^+}$ transport. The

concentration of Li⁺ can vary greatly in the various water areas, so this influence factor can be magnified in the real Li extraction. Therefore, the impact of Li⁺ concentration on its interfacial solvation structure can be schematically illustrated in Figure 4e: this reduction in coordination number lowered the desolvation energy barrier at the interface, thereby accelerating the desolvation process.

2.4. Influence of Force with Other Cations

In addition to Li^+ , the presence of other cations in the seawater (e.g., Na^+ , K^+ , Mg^{2+}) may also influence the solvation structure. Therefore, it is necessary to investigate the roles of these

16163028, 2025, 38, Downloaded from https://adv

.com/doi/10.1002/adfm.202426072 by University Town Of Shenzhen, Wiley Online Library on [18/11/2025]. See the Terms

xonditions) on Wiley Online Library for rules of use; OA articles are governed by the applicable Creative Commons License

www.afm-journal.de

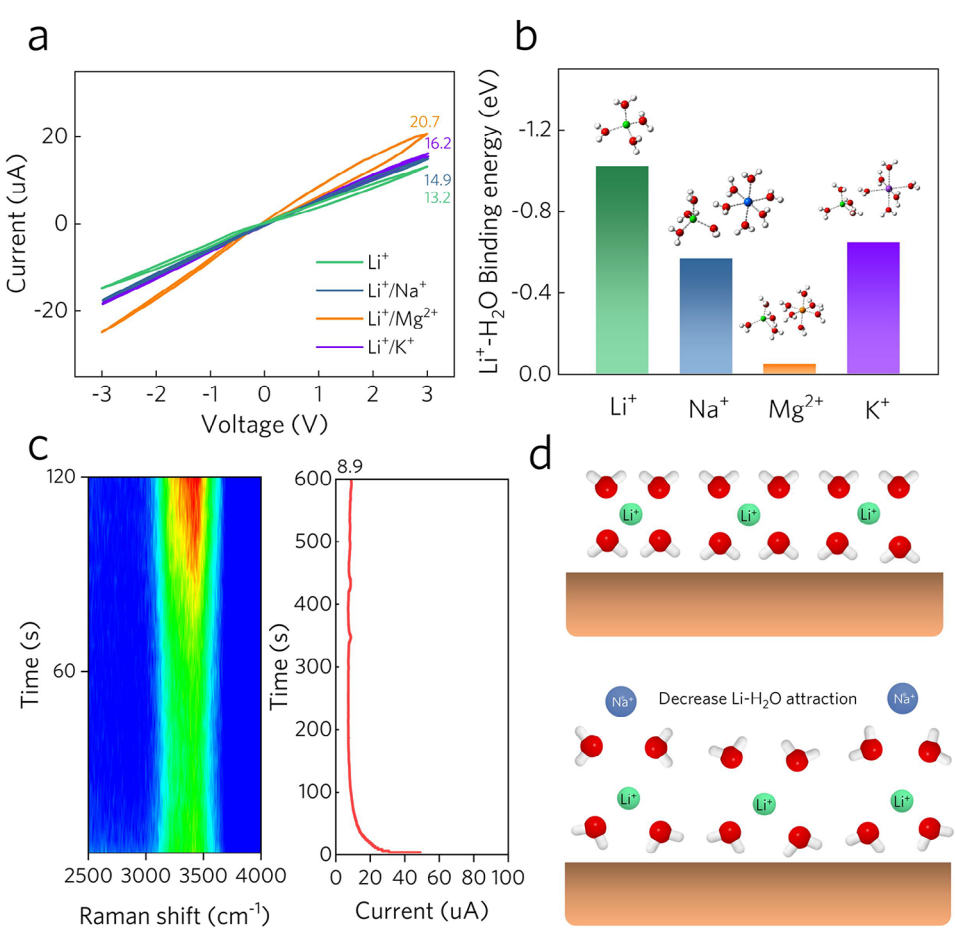


Figure 5. a) CV curves of systems with different cation solutions (1 mol L^{-1} LiCl, 0.5 mol L^{-1} LiCl + 0.5 mol L^{-1} NaCl, 0.5 mol L^{-1} LiCl + 0.5 mol L^{-1} MgCl₂, 0.5 mol L^{-1} LiCl + 0.5 mol L^{-1} KCl) using LLTO-4%LBSO as cation exchange membrane; b) De-solvation energy of Li⁺ for different water cluster structure; c) In situ electrochemical Raman spectra of LLTO in the 0.5 mol L^{-1} LiCl + 0.5 mol L^{-1} NaCl aqueous solution; d) Schematic illustration of other cation force for interfacial water cluster structure.

interfering cations in the desolvation process for Li+. Here, $0.5~M~Li^+ + 0.5~M~X~(X = Na^+,~K^+,~and~Mg^{2+})$ solutions with a total cation concentration of 1 м were prepared. CV tests of these solutions showed that higher current responses can be obtained in the presence of other cations, where Mg²⁺ exhibited the most significant effect while Na⁺ and K⁺ showed similar results (Figure 5a). Calculations of the desolvation energy of Li⁺ in the presence of different cations showed that the introduction of Na+, Mg²⁺, and K⁺ ions all reduced the desolvation energy of Li⁺, with Mg²⁺ causing the most significant reducing effect (Figure 5b). This variation trend aligns with the CV results, suggesting the existence of other metal cations that exhibit stronger interactions with H₂O molecules (Figure S20, Supporting Information) could lead to a weaker solvating effect of Li+. For further analysis, we conducted deep Raman measurements using a pure LLTO pellet with a 0.5 M LiCl + 0.5 M NaCl mixed solution (Figure S21, Supporting Information). Compared to Figure 2a, the results showed weaker Raman peak intensities corresponding to the O-H stretching modes of H₂O (3155 and 3350 cm⁻¹) and the vibrational modes of interactions between water and lithium ions (3540 cm⁻¹) at the interface, and a narrower Raman signal layer corresponding to the accumulation of solvated Li⁺.

In situ electrochemical Raman measurements of 0.5 M LiCl + 0.5 M NaCl mixed solution (Figure 5c) showed that the introduction of Na+ reduced the intensity of the Raman peaks corresponding to solvated Li⁺ at the interface. The current change during voltage application decreased, accompanied by an increased steady-state current, indicating that the introduction of Na+ accelerated the desolvation rate of Li+ at the interface. Additionally, molecular dynamics simulations of different solution phases (Figure S22, Supporting Information) showed that the coordination number of lithium ions in a 1 M LiCl solution was slightly higher than in a 0.5 M LiCl + 0.5 M NaCl mixed solution, both \approx 3.87 at 2.5 Å. Therefore, the improvement in the desolvation process under the introduction of Na⁺ is mainly attributed to the interaction between the Na+ and water clusters, decreasing the desolvation energy of the solvated Li⁺ (Figure 5d). These observations demonstrate that the type of cations in the solution is a key factor influencing the desolvation process of Li⁺.

3. Conclusion

To conclude, in this work, we investigated the impact of the interface between solid electrolyte membranes and aqueous solutions

16163028, 2025, 38, Downloaded

from https://advanced.onlinelibrary.wiley.com/doi/10.1002/adfm.202426072 by University Town Of Shenzhen, Wiley Online Library on [18/11/2025]. See the Terms and Conditions

and-conditions) on Wiley Online Library for rules of use; OA articles are governed by the applicable Creative Commons

ADVANCED
FUNCTIONAL
MATERIALS

on Li+ transport at the solid-liquid interface to achieve efficient and rapid lithium extraction. Employing depth-profiling and in situ Raman spectroscopy techniques, we conducted a comprehensive analysis of the impact of solid surface properties, solute concentrations, and other cations on Li+ desolvation at the interface. Combining multidimensional theoretical calculations, it is found that a more hydrophobic solid electrolyte surface, a higher Li+ concentration, and the presence of cations with strong hydration ability can all reduce the interfacial desolvation energy of Li⁺, leading to more efficient Li separation. By demonstrating how different influencing factors act on the solvation structure at the solid-liquid interface and the desolvation process, this study provides a new pathway for achieving efficient and sustainable Li extraction. It should be noted that the above experiments were based on a two-electrode system with dual Ag/AgCl references which is unsuitable to evaluate the practical seawater treatment efficiency. A four-electrode device is better to monitor the current response. In the future, more quantitative analyses of the correlations between influence factors can be conducted by developing new interface characterization methods, thereby gaining deeper insights into the mechanisms of interfacial Li⁺ transport.

Supporting Information

Supporting Information is available from the Wiley Online Library or from the author.

Acknowledgements

X.Y. and S.C. contributed equally to this work. L. Yang acknowledges the support from the Shenzhen Science and Technology Planning Project (JSGG20220831095604008). Y. Song acknowledges the support from the National Natural Science Foundation of China (No. 52102200).

Conflict of Interest

The authors declare no conflict of interest.

Data Availability Statement

The data that support the findings of this study are available from the corresponding author upon reasonable request.

Keywords

extracting lithium from seawater, Interfacial Li+ transport, raman spectroscopy, solid-liquid interface

Received: December 31, 2024 Revised: March 28, 2025 Published online: April 14, 2025

- [1] J. W. Choi, D. Aurbach, Nat. Rev. Mater. 2016, 1, 16013.
- [2] X. Zeng, M. Li, D. A. El-Hady, W. Alshitari, A. S. Al-Bogami, J. Lu, K. Amine, Adv. Energy Mater. 2019, 9, 1900161.

- [3] Y. Sun, Q. Wang, Y. Wang, R. Yun, X. Xiang, Sep. Purif. Technol. 2021, 256, 117807.
- [4] S. Yang, F. Zhang, H. Ding, P. He, H. Zhou, Joule 2018, 2, 1648.
- [5] C. Liu, Y. Li, D. Lin, P. C. Hsu, B. Liu, G. Yan, T. Wu, Y. Cui, S. Chu, Joule 2020, 4, 1459.
- [6] H. J. Hong, T. Ryu, I. S. Park, M. Kim, J. Shin, B. G. Kim, K. S. Chung, Chem. Eng. J. 2018, 337, 455.
- [7] Z. Meng, M. Wang, X. Cao, T. Wang, Y. Wang, Y. Xu, W. Liu, L. Chen, Y. Huang, X. Liu, Chem. Eng. J. 2022, 445, 136780.
- [8] G. R. Harvianto, S. G. Jeong, C. S. Ju, Korean J. Chem. Eng. 2014, 31, 828
- [9] Y. Steven Kurniawan, R. Rao Sathuluri, K. Ohto, W. Iwasaki, H. Kawakita, S. Morisada, M. Miyazaki, Jumina, Sep. Purif. Technol. 2019, 211, 925.
- [10] N. Choudhary, D. Rajpurohit, A. Saha, S. Yadav, S. Tothadi, B. Ganguly, A. R. Paital, Chem. Eng. J. 2023, 470, 144408.
- [11] X. Zheng, L. Huang, X. Ye, J. Zhang, F. Min, W. Luo, Y. Huang, Chem 2021, 7, 2312.
- [12] Z. Y. Guo, Z. Y. Ji, Q. B. Chen, J. Liu, Y. Y. Zhao, F. Li, Z. Y. Liu, J. S. Yuan, J. Clean. Prod. 2018, 193, 338.
- [13] J. Hu, Y. Jiang, L. Li, Z. Yu, C. Wang, G. Gill, J. Xiao, R. J. Cavagnaro, L. J. Kuo, R. M. Asmussen, D. Lu, ACS Energy Lett. 2022, 7, 2420.
- [14] A. Razmjou, M. Asadnia, E. Hosseini, A. Habibnejad Korayem, V. Chen, Nat. Commun. 2019, 10, 5793.
- [15] H. N. Li, C. Zhang, J. H. Xin, Y. W. Liu, H. C. Yang, C. Y. Zhu, C. Liu, Z. K. Xu, ACS Nano 2024, 18, 2434.
- [16] T. Hoshino, Desalination 2015, 359, 59.
- [17] Y. J. Lim, K. Goh, A. Goto, Y. Zhao, R. Wang, J. Mater. Chem. A 2023, 11, 22551.
- [18] Z. Li, C. Li, X. Liu, L. Cao, P. Li, R. Wei, X. Li, D. Guo, K. W. Huang, Z. Lai, Energy Environ. Sci. 2021, 14, 3152.
- [19] J. Hu, W. Ren, X. Chen, Y. Li, W. Huang, K. Yang, L. Yang, Y. Lin, J. Zheng, F. Pan, Nano Energy 2020, 74, 104864.
- [20] O. Borodin, X. Ren, J. Vatamanu, A. Von Wald Cresce, J. Knap, K. Xu, Acc. Chem. Res. 2017, 50, 2886.
- [21] Z. Chang, H. Yang, Y. Qiao, X. Zhu, P. He, H. Zhou, Adv. Mater. 2022, 34, 2201339.
- [22] Q. Wang, T. Lu, Y. Liu, J. Dai, L. Guan, L. Hou, H. Du, H. Wei, X. Liu, X. Han, Z. Ye, D. Zhang, Y. Wei, H. Zhou, Energy Storage Mater. 2023, 55, 782.
- [23] B. Ren, S. Hu, A. Chen, X. Zhang, H. Wei, J. Jiang, G. Chen, C. Zhi, H. Li, Z. Liu, Adv. Energy Mater. 2024, 14, 2302970.
- [24] X. Zhang, J. Li, H. Ao, D. Liu, L. Shi, C. Wang, Y. Zhu, Y. Qian, Energy Storage Mater. 2020, 30, 337.
- [25] V. Randle, Mater. Charact. 2009, 60, 913.
- [26] Y. Gu, E. M. You, J. De Lin, J. H. Wang, S. H. Luo, R. Y. Zhou, C. J. Zhang, J. L. Yao, H. Y. Li, G. Li, W. W. Wang, Y. Qiao, J. W. Yan, D. Y. Wu, G. K. Liu, L. Zhang, J. F. Li, R. Xu, Z. Q. Tian, Y. Cui, B. W. Mao, *Nat. Commun.* 2023, 14, 3536.
- [27] R. Lv, W. Kou, S. Guo, W. Wu, Y. Zhang, Y. Wang, J. Wang, Angew. Chemie – Int. Ed. 2022, 61, 202114220.
- [28] Y. H. Wang, S. Zheng, W. M. Yang, R. Y. Zhou, Q. F. He, P. Radjenovic, J. C. Dong, S. Li, J. Zheng, Z. L. Yang, G. Attard, F. Pan, Z. Q. Tian, J. F. Li, *Nature* 2021, 600, 81.
- [29] X. Luo, M. Zhou, Z. Luo, T. Shi, L. Li, X. Xie, Y. Sun, X. Cao, M. Long, S. Liang, G. Fang, Energy Storage Mater. 2023, 57, 628.
- [30] H. Ji, Z. Wang, Y. Sun, Y. Zhou, S. Li, J. Zhou, T. Qian, C. Yan, Adv. Mater. 2023, 35, 2208590.
- [31] Y. Wang, Z. Cao, Z. Ma, G. Liu, H. Cheng, Y. Zou, L. Cavallo, Q. Li, J. Ming, ACS Energy Lett. 2023, 8, 1477.